Inhibition of *B. anthracis* Glutamate Racemase by DPA: Discovery of an Allosteric Cryptic Binding Site

Supplementary Information

Katie L. Whalen[1], Kenneth B. Tussey[2], Steven R. Blanke[3,4], and M. Ashley Spies[1,4]*

Department of Biochemistry[1], Program for Biophysics and Computational Biology[2], Department of Microbiology[3], and Institute of Genomic Biology[4], University of Illinois, Urbana, Illinois 61801

Table of Contents

Supplemental Methods..... S2

Supplemental Computational Methods..... S3

Supplemental Results..... S5

Supplemental Tables and Figures..... S6

Supplemental References..... S15

Supplemental Methods

Protein Expression and Purification

A 10 mL starter culture of LB medium with 100 μg/mL ampicillin was prepared from the stock *E. coli* BL21 (DE3) cells containing pET-15b plasmid with the gene of choice and grown overnight at 37 °C with rotation. The 10 mL starter culture was back-diluted into 1 L fresh LB medium with 100 μg/mL ampicillin. Cells were grown at 37 °C with shaking until the optical density at 600 nm reached 0.5-0.8. Protein expression was induced upon addition of a final concentration of 0.1 mM IPTG. Following induction, cells were grown for an additional 16-20 h at 37 °C with shaking (16 °C for mutant proteins). Cells were harvested by centrifugation at 5,000 x *g* for 15 min. Supernatant was discarded and cell pellets were resuspended in bind buffer (50 mM phosphate, 300 mM NaCl, 20 mM imidazole, 0.5 mM Tris carboxyethyl phosphine, pH 8.0). Cell lysis was achieved through sonication (3x 20 sec cycles, 23 kHz and 20 W), using a 100 Sonic Dimembrator from Fisher Scientific. Insoluble materials were pelleted by centrifugation at 30,000 x *g* for 30 min and clarified lysate was applied to 4 mL bed volume of His-Select Cobalt Affinity Gel. Bound protein was washed with 2X 16 mL of wash buffer (50 mM phosphate, 300 mM NaCl, 40mM imidazole, 0.5 mM Tris carboxyethyl phosphine, pH 8.0). Bound protein was eluted twice with 4 mL elution buffer (50 mM phosphate, 300 mM NaCl, 250 mM imidazole, 0.5 mM Tris carboxyethyl phosphine, pH 8.0) and the collected eluant was concentrated via centrifugal filtration. Eluant was incubated at 37 °C for 15 min in the presence of 1 mM ATP and 1 mM $MgCl_2$ to remove molecular weight contaminants suspected to be chaperones. Eluant was then diluted 10X with H_2O and submitted to ion exchange chromatography using a BioRad Uno Q1 column on a BioRad BioLogic DuoFlow HPLC. Pooled fractions were then exchanged into protein storage buffer (50 mM Tris, 100 mM NaCl, 0.2 mM DTT, pH 8.0) and concentrated utilizing a 10,000 MWCO Amicon centrifugal filter device. Finally, protein stocks were stored at a final concentration of 7-10 mg/mL with 20% glycerol at -20 °C.

Colloidal Aggregation Control

Inhibitors were analyzed for the possibility of colloidal aggregation using a previously established detergent-based assay[1] (successfully applied this system to expose colloidal aggregators in Whalen *et al.*[2]). Activity of RacE was measured in the presence and absence of inhibitor in buffer containing 0.01% Triton-X 100 (vol/vol). The percent inhibition was compared to that acquired when conducting the same measurements in buffer without Triton-X 100. If the inhibitor is indeed aggregating, one would expect to see a decrease in the percent inhibition in the presence of detergent (as seen in Whalen *et al.*[2]). Feng and Shoichet stated that a greater than two-fold decrease in inhibition confirms colloidal aggregation[1].

Enzyme Kinetics – Circular Dichroism

Stereoisomerization of D-glutamate by GR was assayed by using a J-720 CD spectropolarimeter from JASCO, Inc. (Easton, MD). A jacketed cylindrical cuvette with a volume of 750 μL and a path length of 10 mm was used for each assay. Readings were measured at 220nm or 225nm depending on contributions to the signal by the inhibitor. All measurements were conducted at 25 ˚C. Concentrations of D-glutamate were varied from 0.25–5 mM in an optically clear borate buffer (50 mM boric acid, 100 mM KCl, 0.7 mM DTT; pH 8.0). Reactions were initiated upon addition of enzyme (approx. 0.5 μM). Data acquisition was performed using a JASCO Spectra Manager v1.54A software and Excel, and fitting and statistical analysis was performed using GraphPad Prism v5.0 (GraphPad Software, Inc., La Jolla, CA).

Monomer:Dimer Equilibrium Model and BN-PAGE Data Fitting

A monomer:dimer equilibrium model was formulated using the following relationships:

$$K_d = \frac{MM}{C} \qquad \text{Eq. 1}$$

$$P_T = M + C \qquad \text{Eq. 2}$$

, where M is the monomer concentration, C is the complex, or dimer, concentration and P_T is the total protein concentration.

$$K_d C = M^2 = (P_T - C)^2 \qquad \text{Eq. 3}$$

Substitution via Eq. 1 and solving for C gives:

$$C = \frac{-\alpha \square \sqrt{\alpha^2 - 4P_T^2}}{2} \qquad \text{Eq. 4}$$

where $\alpha = -2P_T - K_d$. A similar procedure for monomer concentration leads to:

$$M = \frac{K_d + \sqrt{K_d^2 + 4K_d P_T}}{2} \qquad \text{Eq. 5}$$

The *M/C* ratio was measured via pixel quantification of BN-PAGE gels and the total protein concentration is known. The initial value of K_d was set arbitrarily to 0.01 µg/mL and solved by fitting the data. All data fitting was executed using GraphPad Prism v5.0. Additionally, combining equations 3 and 4 leads to the simpler expression in Eq. 6.

$$\frac{M}{C} = \frac{\sqrt{CK_d}}{C} = \frac{K_d}{\sqrt{C}} \qquad \text{Eq. 6}$$

Supplemental Computational Methods

Molecular Dynamic Simulations

The molecular dynamics simulations were performed with the YASARA Structure package version 9.11.9 (YASARA Biosciences)[3]. A periodic simulation cell with boundaries of 99.64 Å, 70.54 Å, and 68.98 Å was employed with explicit solvent , using the dimer (A and B chains) of PDB 2GZM (*B. anthracis* RacE2 GR with ligand D-glu). The AMBER03 force field was used with long-range electrostatic potentials calculated with the Particle Mesh Ewald (PME) method, with a cutoff of 7.864 Å[4-6]. The substrate force field parameters were generated with the AutoSMILES utility[7], which employs semi-empirical AM1 geometry optimization and assignment of charges, followed by assignment of AM1BCC atom and bond types with refinement using RESP charges, and finally the assignments of general AMBER force field atom types. The hydrogen bond network of GR is optimized using the method of Hooft and coworkers[8], in order to address ambiguities from multiple side chain conformations and protonation states that are not resolved by the electron density. YASARA's pKa utility was used to assign pK_a values at pH 7.0[9]. The box was filled with water, with a maximum sum of all bumps per water

of 1.0 Å, and a density of 0.997 g/ml. The simulation cell was neutralized with NaCl (0.9% final concentration; % by mass). Waters were deleted to readjust the solvent density to 0.997 g/ml. A short MD was run on the solvent only. The entire system was then energy minimized using first a steepest descent minimization to remove conformational stress, followed by a simulated annealing minimization until convergence (<0.05 kJ/mol/200 steps). The MD simulation was then initiated, using the NVT ensemble at 298 K, and integration time steps for intramolecular and intermolecular forces every 1.25 fs and 2.5 fs, respectively.

Docking Program Specifications

GOLD employs a traditional genetic algorithm for exploring ligand conformations and binding modes within a partially flexible active site [10]. The GOLD scoring function for ranking binding modes is composed of terms that account for three conditions: hydrogen bonding between ligand and enzyme, the hydrophobic contribution of the energy of binding, and the internal energy of the ligand[10]. Quite contrary, FRED employs a non-stochastic sampling of ligand conformations by systematically rotating and translating conformers within the binding site in a stepwise fashion. Docked complexes are filtered by several default and user-defined constraints, such as the requirement that ligand conformers fit within the active site volume, and then ranked by the scoring function Chemgauss 3. The Chemgauss 3 scoring function is comprised of terms for: steric interactions, ligand hydrogen-bond donors and acceptors, interactions with active site metal atoms, and desolvation[11]. Lastly, AutoDock uses a Lamarckian genetic algorithm to sample ligand conformations and binding modes, which varies slightly from the traditional genetic algorithm employed by GOLD in that conformers are also allowed to search local conformational space to find local minima[12]. AutoDock uses a semiempirical free energy force field to predict free energies of binding which accounts for intermolecular and intramolecular energies, as well as charge-based desolvation.

D-Glu Free Energy Binding Calculations with the Fast Boundary Element Method (BEM)

The method employed here falls under the class of free energy calculations known as Endpoint Methods, which includes the popular MM-PBSA approach. These methods were recently reviewed by Steinbrecher and Labahn[13], and involve calculating ΔG_{bind} from constituent parts of a thermodynamic box that involves solvation of the individual components. The binding energy expression is:

$$\Delta G^{0}_{Bind,Solv} = \Delta G^{0}_{Bind,Vacuum} + \Delta G^{0}_{Solv,Complex} - \left(\Delta G^{0}_{Solv,Ligand} + \Delta G^{0}_{Solv,Receptor}\right) + \Delta G^{0}_{np} \qquad Eq.7$$

In the MM-PBSA method the procedure is based on numerical solution of the differential Poisson equation (also called the finite difference method) and the solvent is represented as a continuum having a relatively high dielectric constant, while the protein and ligand may be viewed as point charges projected onto a grid in a low dielectric continuum. The molecular surface of the protein and ligand is the important interface between these two dielectrics. However, we employ an alternative approach to the finite-difference method called the *Boundary Element Method* (BEM) [14,15]. In this method much of the focus is placed on accurately representing the boundary between the two dielectrics, in which a very accurate boundary charge distribution is used to represent a uniform dielectric at the interface between the low and the high dielectric continuum. From this boundary region of uniform dielectric strength, Coulomb's Law is used to calculate the electrostatic potentials. Each method has distinct strengths and weaknesses, yet the latter has not been as widely employed in the literature even though there have been significant advances in the speed and accuracy of this appraoch[16-18]. The BEM method was designed to perform optimally for such curved protein surfaces, by accurately representing the geometry of the protein boundaries. The work of Zauhar and Morgan[19] have shown that the geometry of the boundary region is of central importance to representing the electrostatic potential of proteins[15], and may avoid some of the difficulties inherent in assignment of the protein dielectric in the finite difference approach of MM-PBSA (recently

reviewed by Warshel and co-workers[20]). A major difficulty in Endpoint methods is assigning an internal dielectric. Here we used a wide range of values for ε_p, which did not affect the relative binding energies or the trends seen in Fig. 5d, but only the absolute free energies of binding. It is important to note that $\Delta G_{binding}$ values obtained from Endpoint methods, such as MM-PBSA or BEM, should be viewed as accurate scoring functions, which have enhanced rank-ordering value, rather than as metrics of accurate absolute binding free energy[21]. For the current study, BEM, the boundary between solvent (dielectric constant 78) and solute (dielectric constant ranged from 2 to 28) was formed by the latter's molecular surface, constructed with a solvent probe radius of 1.4 Å and the following radii for the solute elements: polar hydrogens 0.32 Å, other hydrogens 1.017 Å, carbon 1.8 Å, oxygen 1.344 Å, nitrogen 1.14 Å, sulfur 2.0 Å. The solute charges were assigned based on the AMBER03 force field[22], using GAFF/AM1BCC[23] for the ligands. The term for the hydrophobic component of ligand binding, ΔG_{np} was calculated by using the empirical treatment of Tan *et al.*[24] (SAV probe = 1.80 Å, surface tension (ɣ) = 0.0480 kcal/mol-Å^3, and constant offset (c) = -3.2655 kcal/mol.).

Supplemental Results

Monomer versus Dimer Docking

DPA was docked to the same site with only a single monomer present using AutoDock and showed severely attenuated binding affinity (Interaction Energy = -27.45 kcal/mol (dimer) versus -14.81 kcal/mol (monomer), calculated by LigX[25]).

Hydrogen-Bond Network of Active Site

In E_2·D-glu_2, the distance between the side chain of Thr186 and His187 and the amine of glutamate was 4.34 Å and 5.32 Å, respectively. For E_2·D-glu_2·DPA, the distance between Thr186 and His187 and the amine was 2.99 Å and 3.77 Å, respectively. Thus, only in E_2·D-glu_2·DPA is Thr186 within hydrogen-bonding distance of the substrate. In addition to increased contact with glutamate, the movement of Thr186 brings the side chain hydroxyl within hydrogen-bonding distance of Ala73 of an adjacent loop. This hydrogen bond may be responsible for bringing both the side chain and backbone amines of Asn75 close enough to glutamate to form hydrogen bonds with either oxygen of its α carboxylate (3.59 Å and 2.92 Å, respectively), interactions that are completely absent in the E_2·D-glu_2 (6.50 Å and 4.99 Å, respectively).

Structures were critically analyzed to find the source of the weaker free energy of binding of monomer A of E_2·D-glu_2·DPA. It was previously reported that a main conformational change related to glutamate binding occurs in a loop containing His187 and Thr186 which have both been indicated in binding and catalysis[26]. Thus, we began by examining the effect of DPA binding on this loop. Ligand interaction mapping of equilibrated E_2·D-glu_2·DPA after the 20 nanosecond simulation show two water bridges formed between DPA and Asp210 and Glu211 of the A monomer of RacE2 (**Fig. 5c**). Asp 210 goes on to form a hydrogen bond with the side-chain hydroxyl of Ser207 (previously implicated in DPA binding by initial ligand interaction mapping of the top-docked complex prior to MD). Ser207 also forms a water bridge with Glu211. This complex network of direct hydrogen bonds and water bridges between DPA and the A monomer occurs twenty residues downstream of the catalytic residues, separated by a short α-helix and β-sheet. It is possible then that interactions between DPA and Ser207, Asp210 and Glu211 result in a rearrangement in the enzyme conformation that is translated down the backbone to the catalytic residues, His187 and Thr186.

Solvation and DPA Inhibition

An additional water molecule interacting with glutamate of the E_2·D-glu_2·DPA further indicates an active site rearrangement coincident with binding of DPA. The active site solvent accessible volume for the E_2·D-glu_2 monomer A is 1214.35 $Å^3$ which decreases to 1171.15 $Å^3$ for the E_2·D-glu_2·DPA monomer A, a difference of 43.2 $Å^3$. Thus, the additional water bridge seen in E_2·D-glu_2·DPA is not due to more water molecules in the active site but instead more optimal positioning of present water molecules. Thus, greater protein solvation energy of E_2·D-glu_2·DPA appears to contribute at least partially to the source of the weaker D-glu binding free energy.

Monomer-Monomer Interactions

According to the equilibrated structure resulting from MD simulation, binding of DPA to the RacE2 dimer interface disrupts two inter-monomer hydrogen bonds occurring between Lys106a and Asp210b (and vice versa, Lys106b to Asp210a), forcing either Lys106 to instead hydrogen bond to Glu211. There is no net loss of direct contact between the monomers with DPA bound, which agrees well with the results of Blue Native PAGE.

Supplementary Tables and Figures

Supplementary Table 1. Fitting parameters of RacE2_WT activity versus DPA data to varying inhibition models via GraphPad Prism v5.0.

Inhibition Model	Degrees of Freedom	Abs. Sum of Squares
Competitive	13	0.001858
Noncompetitive	13	0.0009267
Uncompetitive	13	0.001597
Mixed Model	12	0.0009108

Supplementary Table 2. Comparison of global fitting via F test of RacE2_WT activity versus DPA data to varying inhibition models.

Parameter	Comparison 1	Comparison 2	Comparison 3
Null Hypothesis	Competitive Inhibition	Uncompetitive Inhibition	Noncompetitive Inhibtion
Alternative Hypothesis	Mixed Model Inhibition	Mixed Model Inhibition	Mixed Model Inhibition
P Value	0.0041	0.0109	0.6548
Conclusion (alpha = 0.05)	Reject Null	Reject Null	Do Not Reject Null
Preferred Model	Mixed Model Inhibition	Mixed Model Inhibition	Noncompetitive Inhibition
F (DFn, DFd)	12.48 (1,12)	9.037 (1,12)	0.2102 (1,12)

Supplementary Table 3. Steady-state kinetic parameters of WT and mutant RacE2 enzymes as determined by circular dichroism. Fit to the Michaelis-Menten equation via GraphPad Prism v5.0.

Protein	D → L Racemization		
	k_{cat} (s^{-1})	K_m (mM)	k_{cat}/K_m (10^3 M^{-1} s^{-1})
RacE2 WT	2.13 ± 0.1	1.27 ± 0.3	1.68 ± 0.2
RacE2 K106A	5.68 ± 0.8	2.27 ± 0.7	2.50 ± 0.3
RacE2 S207A	0.73 ± 0.1	0.29 ± 0.1	2.52 ± 0.4

Gene	Desired Mutation	Primer	Primer Sequence (5'→3')
racE2	Lys106Ala	K106Afor	5'-agttattcacccaggatcacgtacagctttagcagtgacaaacacatac-3'
		K106Arev	5'-gtatgtgtttgtcactgctaaagctgtacgtgatcctgggtgaataact-3'
racE2	Ser207Ala	S207Afor	5'-ggagataaagtacaactcattgcttcaggtgatgaaacagcgc-3'
		S207Arev	5'-gcgctgtttcatcacctgaagcaatgagttgtactttatctcc-3'

Supplementary Table 4. Description of primers used for site-directed mutagenesis of *racE2*.

Supplementary Table 5. Comparison of global fitting via F test of RacE1_WT activity versus DPA data to varying inhibition models.

Parameter	Comparison 1	Comparison 2	Comparison 3
Null Hypothesis	Competitive Inhibition	Uncompetitive Inhibition	Noncompetitive Inhibtion
Alternative Hypothesis	Mixed Model Inhibition	Mixed Model Inhibition	Mixed Model Inhibition
P Value	0.0221	0.0484	0.6915
Conclusion (alpha = 0.05)	Reject Null	Reject Null	Do Not Reject Null
Preferred Model	Mixed Model Inhibition	Mixed Model Inhibition	Noncompetitive Inhibition
F (DFn, DFd)	6.156 (1,20)	4.418 (1,20)	0.1621 (1,20)

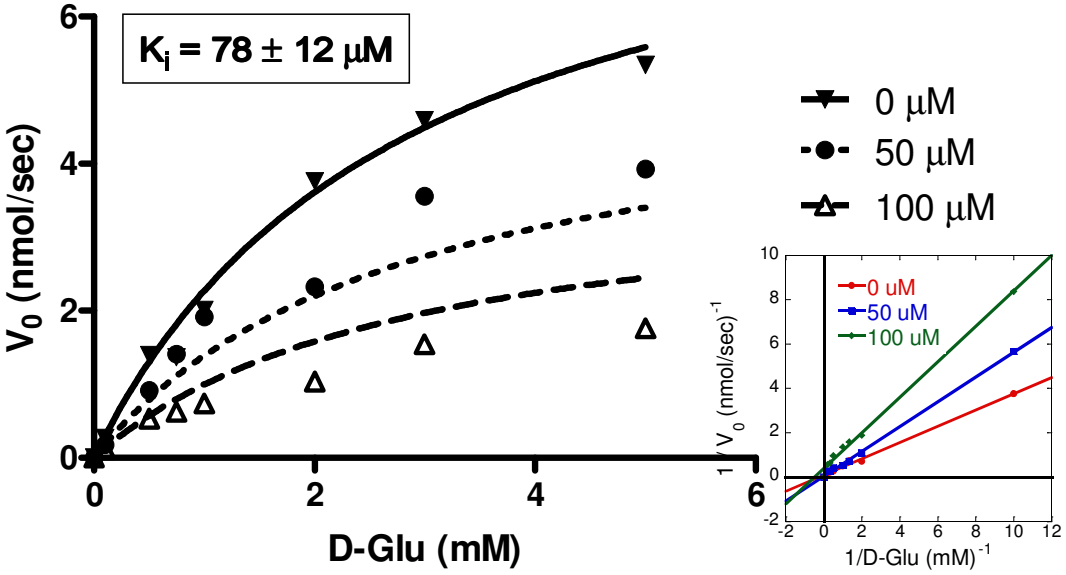

Supplementary Figure 1. Inhibition of RacE1 by DPA assayed via circular dichroism and globally fit to a noncompetitive inhibition model, resulting in a K_i value of 78 ± 12 μM.

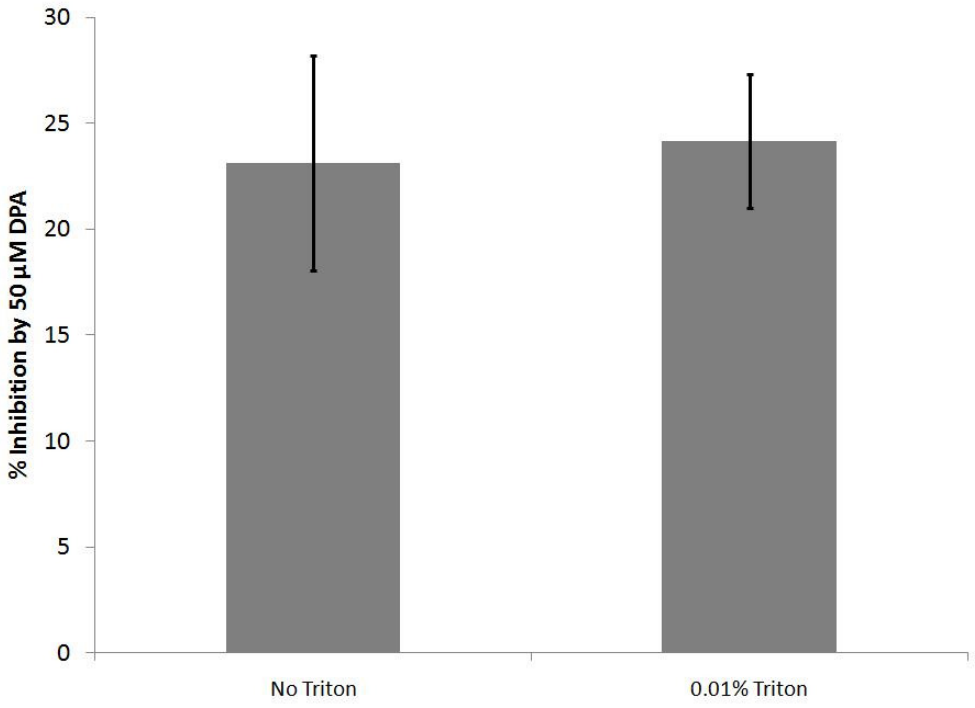

Supplementary Figure 2. Colloidal aggregate test for false positives. Inhibition of RacE2 by 50 µM DPA was assayed in the presence and absence of 0.01% Triton-X 100 detergent. The percent inhibitions of either set of conditions were within error (< 10%) proving DPA not to act through aggregate formation. Data represents the average of three separate trials with standard deviation shown.

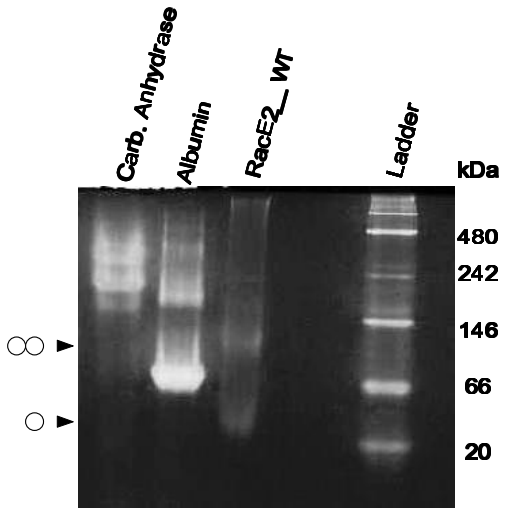

Supplementary Figure 3. Blue Native PAGE of WT RacE2 and running controls with NativeMark ladder (10% resolving gel, 4% stacking gel). Monomer band appears to migrate slightly slower than the 20 kDa marker, as expected (RacE2 monomer MW = 30 kDa). Dimer band appears to migrate slightly slower than the 66 kDa marker (RacE2 dimer MW = 60 kDa) which is most likely due to the fact that the RacE2 homodimer has a more elongated oval shape (see diagram adjacent to arrow head) than the globular marker protein, and thus migrates slower. Higher order oligomers are also present on the gel in negligible quantities.

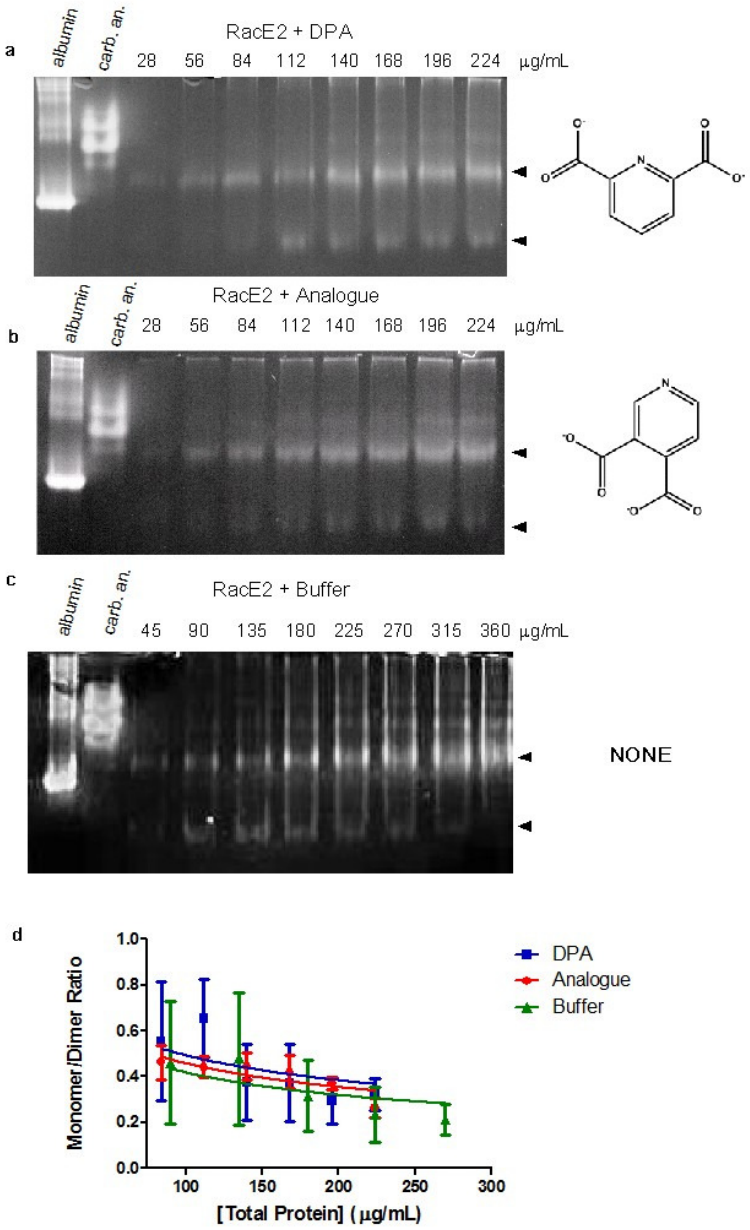

Supplementary Figure 4. BN-PAGE to determine the effect of DPA on RacE2 dimerization. Loading buffer, running buffer and PAGE gel contained 1 mM DPA (**a**) , 1mM 3,4-pyridinedicarboxylic acid (**b**), or buffer (**c**). Albumin and carbonic anhydrase were included as running controls. Arrowheads indicate bands representing the dimer and monomer. Band intensity was quantified via pixel counting and the ratio of monomer to dimer was fitted to an expression for monomer:dimer equilibrium (derivation of expression detailed above in Supplementary Methods). Data represents an average of two or more independent trials with standard error shown. Fitting of data resulted in the following K_d values for RacE2 in the presence of DPA, analogue, or buffer: 48 ± 13, 39 ± 5, and 30 ± 7 µg/mL, respectively. Thus, BN-PAGE would confirm that there is no significant change in the K_d of dimerization due to the presence of DPA.

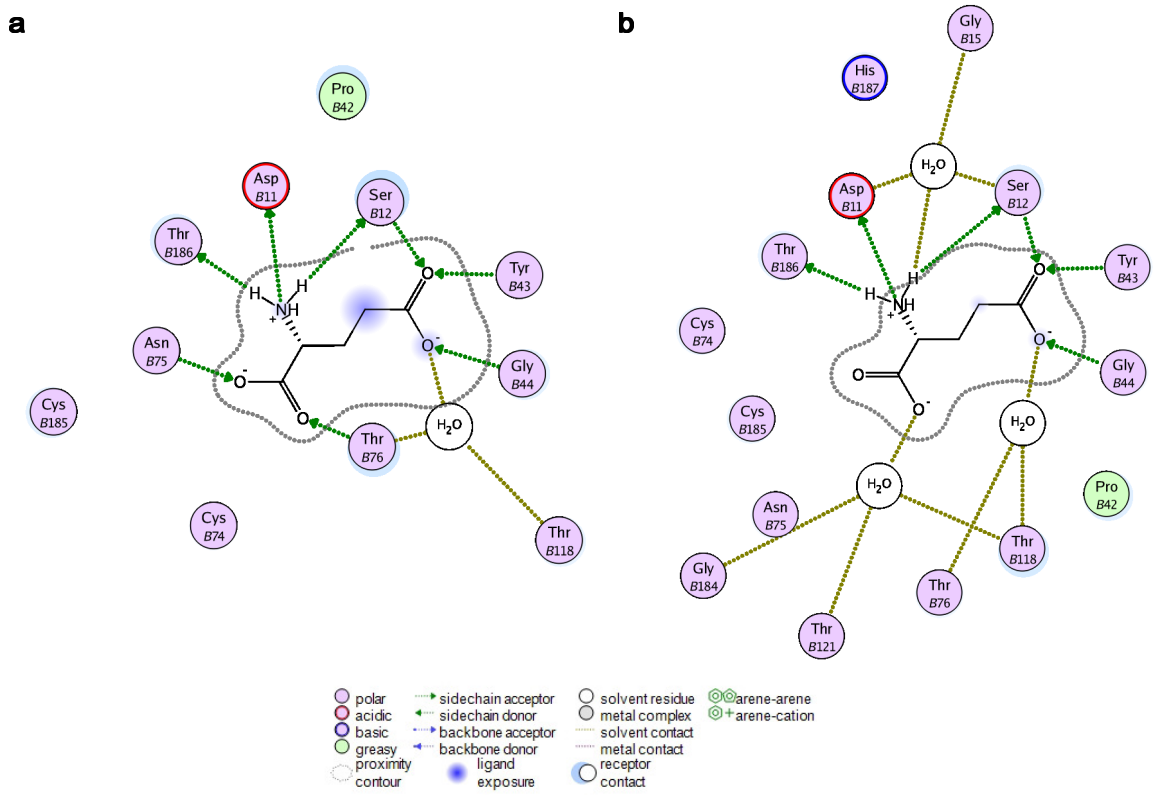

Supplementary Figure 5. Ligand interaction maps for glutamate bound to the active site of monomer B when DPA is absent (**a**) and bound (**b**). Maps were constructed from the equilibrated structures of the 20 nanosecond MD simulations.

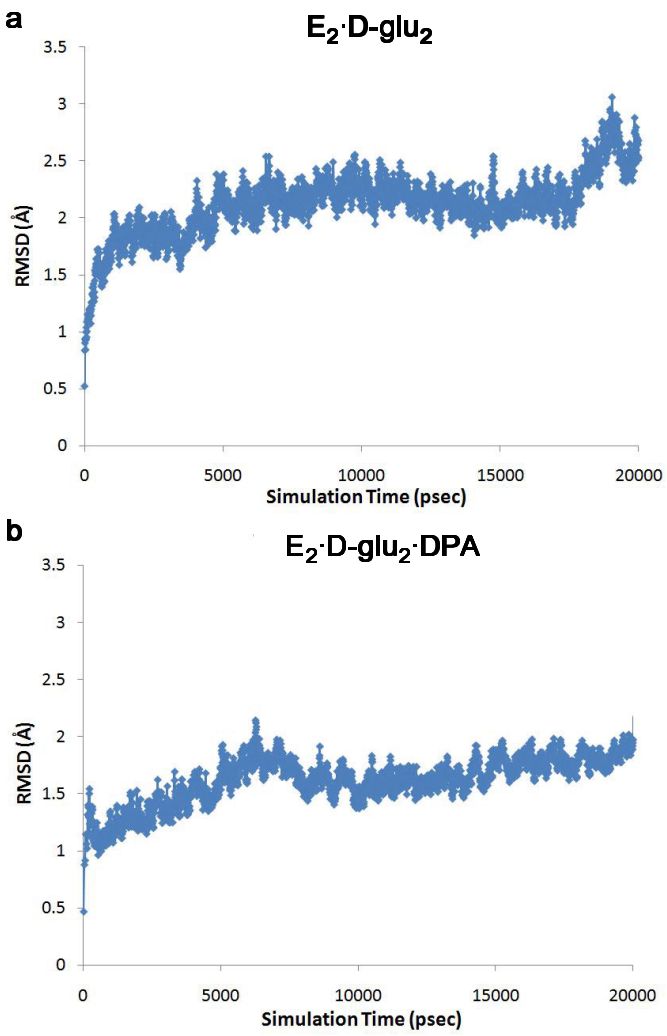

Supplementary Figure 6. Equilibration achieved over 20 nanoseconds of molecular dynamics simulations. Differences between the backbone carbons of each subsequent simulation snapshot structure and the original structure, expressed as RMSD (Å), plotted against time for the E_2·D-glu_2 (**a**) and E_2·D-glu_2·DPA complex (**b**).

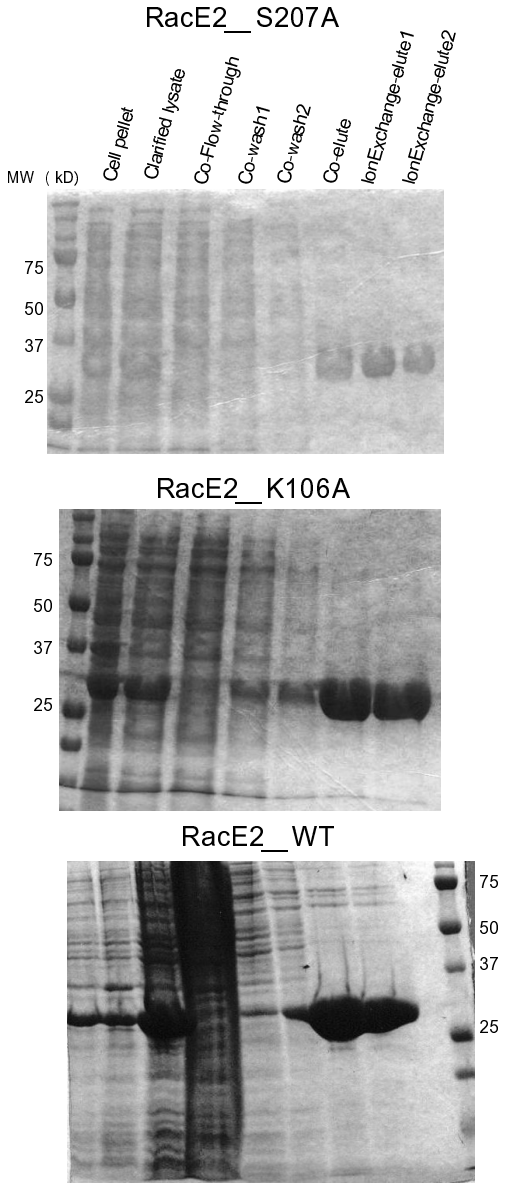

Supplementary Figure 7. Purification of recombinant 6x-His-tagged RacE2_S207A, RacE2_K106A, and WT RacE2 via Co^{2+}-affinity chromatography followed by UNO-Q anion-exchange chromatography.

Supplementary References

(1) Feng, B. Y.; Shoichet, B. K. *National Protocols* **2006**, *1*, 550.

(2) Whalen, K. L.; Pankow, K. L.; Blanke, S. R.; Spies, M. A. *ACS Medicinal Chemistry Letters* **2010**, *8*, 9.

(3) Krieger, E.; Koraimann, G.; Vriend, G. *Proteins: Structure, Function, and Genetics* **2002**, *47*, 393.

(4) Cornell, W. D.; Cieplak, P.; Bayly, C. I.; Gould, I. R.; Merz, K. M., Jr.; Ferguson, D. M.; Spellmeyer, D. C.; Fox, T.; Caldwell, J.; Kollman, P. A. *Journal of the American Chemical Society* **1995**, *117*, 5179.

(5) Duan, Y.; Wu, C.; Chowdhury, S.; Lee, M. C.; Xiong, G.; Zhang, W.; Yang, R.; Cieplak, P.; Luo, R.; Lee, T.; Caldwell, J.; Wang, J.; Kollman, P. *Journal of Computational Chemistry* **2003**, *24*, 1999.

(6) Essmann, U.; Perera, L.; Berkowitz, M. L.; Darden, T.; Lee, H.; Pedersen, L. G. *Journal of Chemical Physics* **1995**, *103*, 8577.

(7) Jakalian, A.; Jack, D. B.; Bayly, C. I. *Journal of Computational Chemistry* **2002**, *23*.

(8) Hooft, R. W. W.; Vriend, G.; Sander, C.; Abola, E. E. *Nature* **1996**, *381*, 272.

(9) Krieger, E.; Nielsen, J. E.; Spronk, C. A. E. M.; Vriend, G. *Journal of Molecular Graphics and Modeling* **2006**, *25*, 481.

(10) Jones, G.; Willett, P.; Glen, R. C.; Leach, A. R.; Taylor, R. *Journal of Molecular Biology* **1997**, *267*, 727.

(11) McGann, M. R.; Almond, H. R.; Nicholls, A.; Grant, J. A.; Brown, F. K. *Biopolymers* **2003**, *68*, 76.

(12) Morris, G. M.; Goodsell, D. S.; Halliday, R. S.; Huey, R.; Hart, W. E.; Belew, R. K.; Olson, A. J. *Journal of Computational Chemistry* **1998**, *19*, 1639.

(13) Steinbrecher, T.; Andreas, L. *current Medicinal Chemistry* **2010**, *17*, 767.

(14) Juffer, A. H.; Botta, E. F. F.; Vankeulen, B. A. M.; Vanderploeg, A.; Berendsen, H. J. C. *Journal of Computational Physics* **1991**, *97*, 144.

(15) Zauhar, R. J.; Morgan, R. S.; Shaw, P. B. *Biophysical Journal* **1985**, *47*, A21.

(16) Chan, S. L.; Purisima, E. O. *Computers & Graphics* **1998**, *22*, 83.

(17) Purisima, E. O. *Journal of Computational Chemistry* **1998**, *19*, 1494.

(18) Totrov, M.; Abagyan, R. *Biopolymers* **2001**, *60*, 124.

(19) Zauhar, R. J.; Morgan, R. S. *Journal of Molecular Biology* **1985**, *186*, 815.

(20) Kato, M.; Braun-Sand, S.; Warshel, A.; Stroud, R.; Finer-Moore, J. Challenges and progresses in calculations of binding free energies - what does it take to quantify electrostatic contributions to protein-ligand interactions. In *Computational and structural approaches to drug discovery : ligand-protein interactions*; RSC Publishing: Cambridge, 2008; pp 268.

(21) Shirts, M. R.; Mobley, D. L.; Brown, S. P.; Merz, K. M.; Ringe, D.; Reynolds, C. H. Free-energy calculations in structure-based drug design. In *Drug design : structure- and ligand-based approaches*; Cambridge University Press: Cambridge [U.K.] ; New York, 2010; pp 61.

(22) Duan, Y.; Wu, C.; Chowdhury, S.; Lee, M. C.; Xiong, G. M.; Zhang, W.; Yang, R.; Cieplak, P.; Luo, R.; Lee, T.; Caldwell, J.; Wang, J. M.; Kollman, P. *Journal of Computational Chemistry* **2003**, *24*, 1999.

(23) Wang, J. M.; Wolf, R. M.; Caldwell, J. W.; Kollman, P. A.; Case, D. A. *Journal of Computational Chemistry* **2004**, *25*, 1157.

(24) Tan, C.; Tan, Y.-H.; Luo, R. *Journal of Physical Chemistry B* **2007**, *111*, 12263.

(25) Molecular Operating Environment; 2008.10 ed.; Chemical Computing Group: Montreal, Quebec, Canada.

(26) Ruzheinikov, S. N.; Taal, M. A.; Sedelnikova, S. E.; Baker, P. J.; Rice, D. W. *Structure* **2005**, *13*, 1707.